Journal of Geochemical Exploration 198 (2019) 123–131

Contents lists available at ScienceDirect

Journal of Geochemical Exploration

journal homepage: www.elsevier.com/locate/gexplo

# LLHR-type chalcopyrite Re-Os geochronology and geochemistry of the Xiaotongchang Cu deposit in south Ailaoshan and its geological significances

Wenjun Li[a,b,c], Bingyu Gao[a,b,c], Lianchang Zhang[a,b,c,*], Xindi Jin[a,b], Patrick Asamoah Sakyi[d]

[a] Key Laboratory of Mineral Resources, Institute of Geology and Geophysics, Chinese Academy of Sciences, Beijing 100029, China
[b] Institutions of Earth Science, Chinese Academy of Sciences, Beijing 100029, China
[c] University of Chinese Academy of Sciences, Beijing 100049, China
[d] Department of Earth Science, University of Ghana, P. O. Box LG 58, Legon-Accra, Ghana

ARTICLE INFO

*Keywords:*
Xiaotongchang Cu deposit
LLHR
Chalcopyrite
Re-Os isotopic age
Ailaoshan orogenic belt

ABSTRACT

The Xiaotongchang Cu deposit is located in the south Ailaoshan and at the contact between Yunnan province of China and Vietnam. Four Cu ore bodies are distributed parallel to each other in an interlayer fracture zone in the Permian Emeishan basalt. The major ore mineral in the deposit is chalcopyrite, and the main gangue minerals are quartz and calcite. New Re-Os data for chalcopyrite from the Xiaotongchang Cu deposit show tens of ppb Re abundances (1–86 ppb) and contain essentially no common Os. All the samples have extremely high $^{187}Re/^{188}Os$ (up to $2.3 \times 10^4$), and the dominance of radiogenic Os and high $^{187}Re/^{188}Os$ are diagnostic features of "LLHR" (low-level, highly radiogenic) sulfides. The Re-Os isochrone age for the No. 1 and No. 3 Cu bodies show that the phase of Cu mineralization predominantly occurred in the Middle Triassic, with an age of 230.6 ± 1.1 Ma. Thus, the mineralization occurred much later than the periods of major eruption of the Emeishan large igneous provinces, indicating a closer relationship with the late collisional processes in the Ailaoshan orogenic belt. Combined with REEs patterns and consistently positive $\delta^{34}S$ values (7.4–9.2‰), it can be concluded that the ore-forming materials of the Cu deposit are derived from a mixture of mantle and crust components.

## 1. Introduction

Re-Os isotope system has long been recognized as an effective tool to trace the origin of metals and directly dating mineralization (Nozaki et al., 2010; Ying et al., 2014; Zhang et al., 2016; Kelley et al., 2017; Zhou et al., 2017; Huang et al., 2018). Molybdnite ($MoS_2$) is ideal for dating using Re-Os isotope system, but recently geologists are focused on Re-Os geochronology of sulfides with low Re and Os abundances. Re-Os dating of chalcopyrite is widely used to obtain metallogenic age directly and provide an important factor to understand the relationship between the ore-forming processes and regional tectonic evolution (Zeng et al., 2014; Wang et al., 2015; Torgersen et al., 2015; Deng et al., 2016).

The Ailaoshan metallogenic belt is located in the south-central part of the Yunnan Province near the Vietnam which is the part of the junction of the Tethyan tectonic domain and Yangzi tectonic domain (Ge et al., 2010; Yuan et al., 2010). The Jinping Cu—Ni subzone is located in the south of the Ailaoshan metallogenic belt. These deposits can be classified into three types. Type one is porphyry-type deposit (i.e. Tongchang Cu deposit, Machangqing Cu deposit and Changan Cu—Mo deposit), formed during 37–32 Ma (He et al., 2011; Zhang et al., 2014). The second type is copper-nickel sulfide deposit, such as Baimazhai Cu—Ni sulfide deposit, and the mineralization epoch of this deposit type was 259 Ma (Shi et al., 2006). The last type is vein Cu deposit in basalts (i.e. Xiaotongchang Cu deposit and Mengla Cu deposit), which is mainly hosted in the interlayer fracture zone of the basalt (Yang and Wang, 2012; Luo et al., 2011; Xiao et al., 2003; Li, 2009). Many studies have focused on the dating of the porphyry-type and the copper-nickel sulfide deposits mentioned above. Whereas, the vein Cu deposit in this area has received little attention, and due to lack of data on geochemistry and chronology, the relevant knowledge of ore-forming process and regularity is scarce.

The studied Xiaotongchang deposit is a typical Cu vein deposit in Jinping area, SW Yunnan province (Chen, 2015; Dai et al., 2004; Shen, 2013). Dai et al. (2004) and Chen (2015) were focused on the relationship between copper deposits and Emeishan basalt. Shen (2013)

* Corresponding author at: Key Laboratory of Mineral Resources, Institute of Geology and Geophysics, Chinese Academy of Sciences, Beijing 100029, China.
*E-mail address:* lczhang@mail.igcas.ac.cn (L. Zhang).

https://doi.org/10.1016/j.gexplo.2018.11.011
Received 10 April 2018; Received in revised form 31 July 2018; Accepted 26 November 2018
Available online 28 November 2018
0375-6742/ 

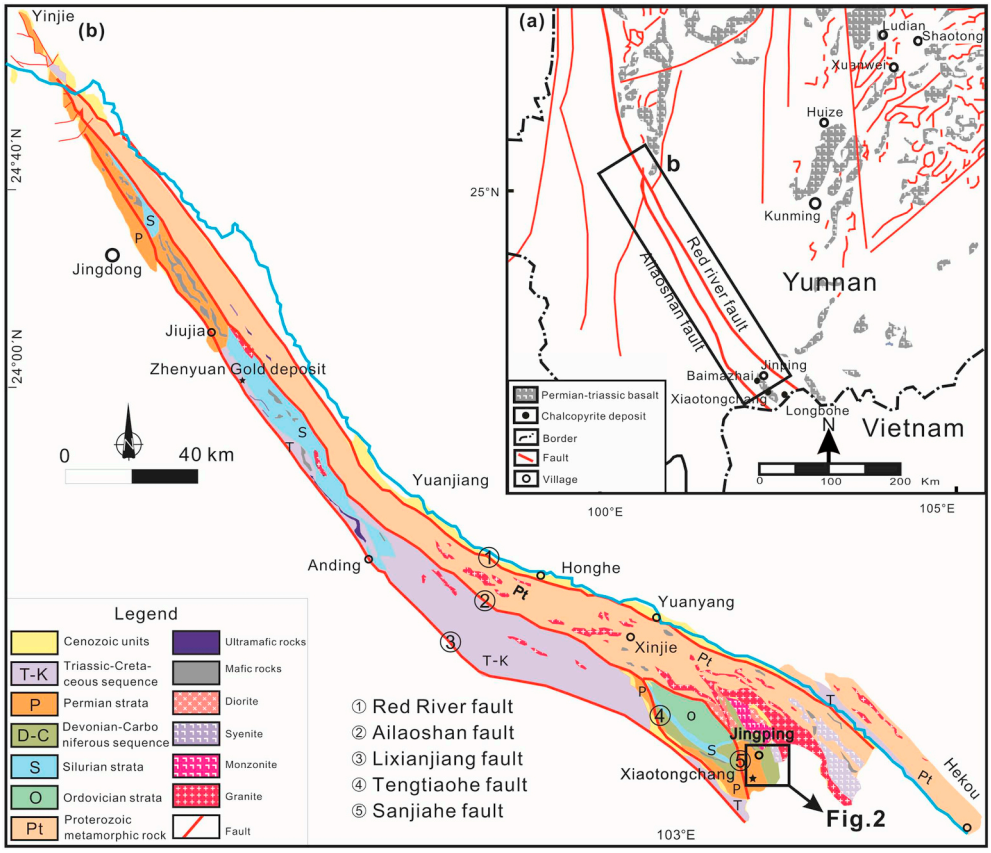


**Fig. 1.** (a) Geological sketch map showing the distribution of the Ailaoshan orogen Belt and Emeishan Volcanic Province (modified after Xu et al., 2007); (b) geological map of the Ailaoshan Belt (modified after Cai et al., 2014).

studied the deposit geological characteristics and stable isotope C and S, then preliminarily analyzed the genesis of the deposit. Previous work was focused on the geological context and lack of geochronology evidence. Here, the chalcopyrite in Xiaotongchang deposit is first attempt to directly date the Cu ore-forming age by Re-Os isotopes. This paper is focused on Re-Os dating of chalcopyrite and the S, REEs geochemistry of the Xiaotongchang Cu deposit to initiate further discussion on the timing of the ore formation and provide additional information for regional metallogenic regularity and tectonic evolution.

## 2. Geological setting

### 2.1. Regional geology

The Jinping block is located to the south of Yangtze craton (Fig. 1a), on the southern section of Ailaoshan metallogenic belt and on the west side of Red-river fault (Fig. 1b). The strata occurring in the Jinping block include Ordovician to Tertiary. The Ordovician strata distribute in the central and eastern parts which are composed of shale, arcose, quartz and stone. The Silurian system unconformity overlies the Ordovician rocks, consisting of dolostone, shale and slate. The Devonian and Carboniferous sedimentary rocks are characterized by limestone and dolostone. Permian and Triassic are found in the Laoxun-Xiaotongchang area, the lower part of the Permian strata are developed, which are mainly consisted of the limestone, and Triassic strata are mainly composed of limestone and limy dolomite (Fig. 2).

The extensive Permian Emeishan basalts are exposed over the Jinping area, from SW of Jinping County to the western side of Mengla County (Fig. 2). The thickest basalt sequence, measuring ~4500 m, occurs in Dalaotang of southwestern Jinping. The lithology is mainly composed of porphyritic basalt, amygdaloidal basalt, dense massive basalt and trachy basalt.

### 2.2. Deposit geology

The exposed strata in the Xiaotongchang area include mainly the early Permian Emeishan basalt, late Triassic black shale, siltstone and early Permian limestone in the Maokou Formation (Fig. 3). The ore bodies are mainly controlled by NW-trending interlayer fracture zone. The Xiaotongchang Cu deposit is mainly composed of four Cu ore bodies, including the NW-trending No. 1 to No. 4 ore bodies, parallel occurring within interlayer fracture zone in Permian Emeishan basalt (Fig. 3). Some basic parameters of the No. 1 and No. 3 ore bodies are as follows: The ore bodies are variable in size from 700 to 300 m long, 2.0 to 10.7 m thick, and 100–200 m in vertical extend. The copper grade has large variation, from 0.4% to 20%. Ore minerals are mainly of chalcopyrite, which is either massive or occurs as vein, accompanied by quartz and calcite in the interlayer fracture zone.

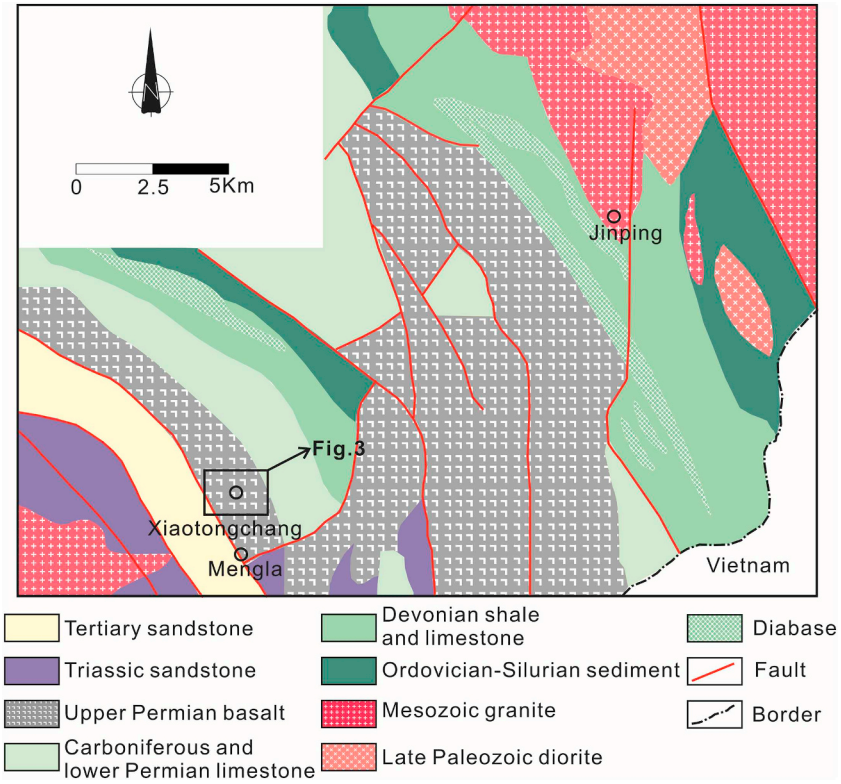


**Fig. 2.** Regional geological map of Jinping area in the Ailaoshan Belt (modified after Xiao et al., 2003).

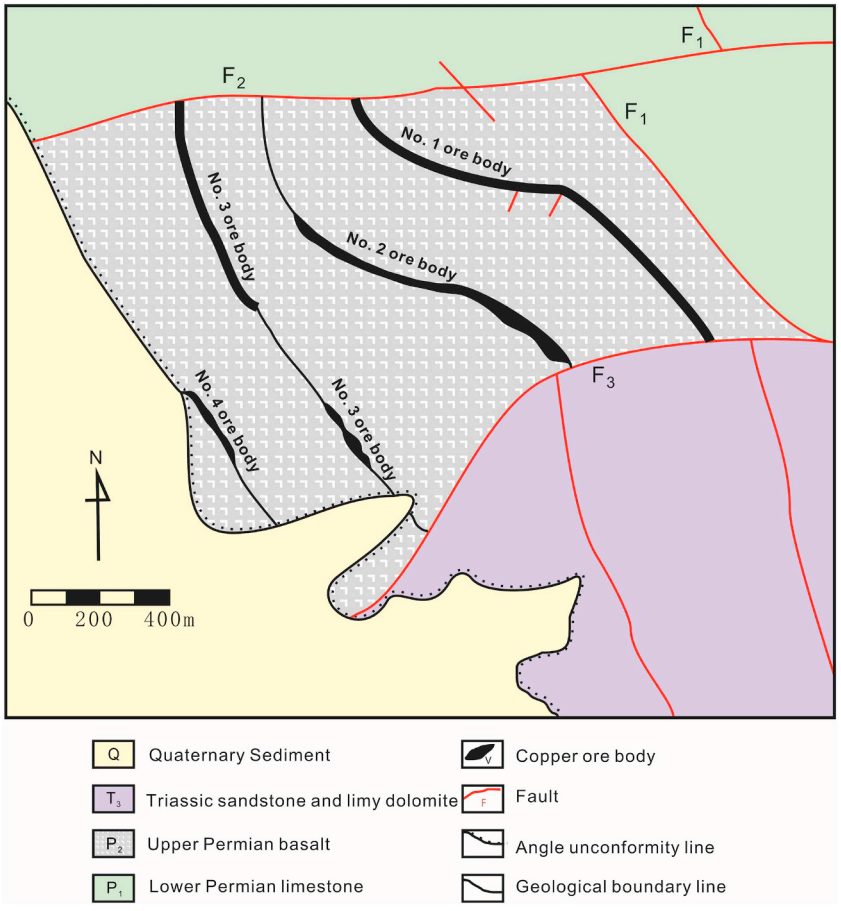


**Fig. 3.** Geological map of the Xiaotongchang copper deposit in Jinping area (Modified from Shen (2013)).

The ores from the No. 1 ore body have a mineral assemblage of chalcopyrite, quartz and minor calcite (Fig. 4a).The chalcopyrite occurs among the euhedral-subhedral quartz (Fig. 4b). Major ore mineral in the No. 3 ore body is chalcopyrite, existing in the massive ore type (Fig. 4d). Gangue minerals include 85–95% euhedral calcite with less xenomorphic, fine-grained quartz (Fig. 4e). Interestingly, the No. 1 Cu ore body has a higher grade than in No. 3.Associated minerals in latter are mainly calcite and less quartz, in contrast to quartz being the primary mineral in No. 1 ore body with little calcite.

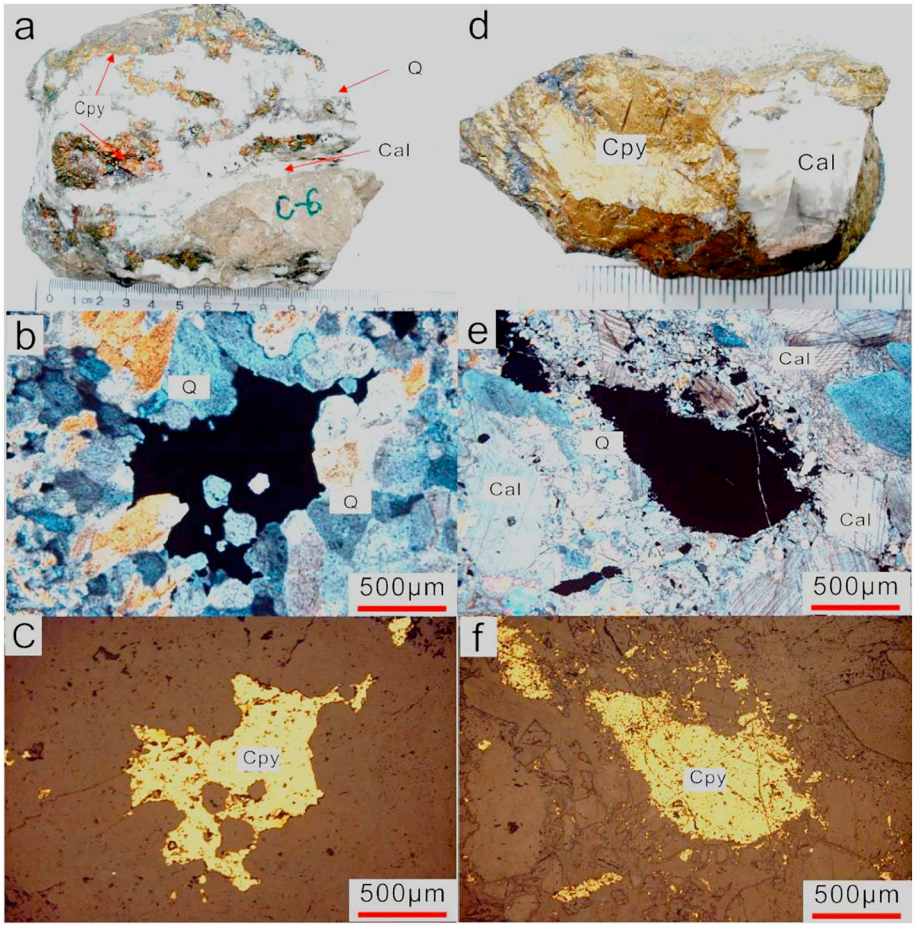


**Fig. 4.** Specimen photos and photomicrographs of chalcopyrite sample from No. 1 (a–c) and No. 3 (d–f) ore bodies in the Xiaotongchang deposit. Abbreviations: Cpy = chalcopyrite; Q = quartz; Cal = calcite.

## 3. Sampling and analytical techniques

Samples used in this study came from two locations. Samples (XTC1) from the No. 1 ore body in the Xiaotongchang deposit represent low-grade sulfide zones associated with quartz and less calcite. Samples (XTC3) from the No. 3 ore body represent high-grade sulfide zones accompanied by mainly calcite. Six chalcopyrite samples from the No. 1 ore body separates weighing about 2–5 g were obtained using traditional isolation methods (crushing, magnetic and handpicking) whereas five chalcopyrite samples from No. 3 were crushed to a mesh size of 2 mm, after which the mineral grains were handpicked under a binocular microscope. All the chalcopyrite samples were selected for Re-Os dating, sulfur isotope analysis and trace elements determination. Three basalt samples were collected for the trace elements determination. Besides these, fluid inclusions in quartz and calcite separates from five Cu-bearing samples in both ore bodies were analyzed for their $Cl^-$ content. All the geochemical analyses were performed at the Institute of Geology and Geophysics, Chinese Academy of Sciences in Beijing.

### 3.1. Re-Os isotope analysis

The modified version of the Carius tube method was used for the Re-Os analysis of chalcopyrite. Details can be found in Jin et al. (2013). In brief, approximately 1 g of each chalcopyrite was weighted and loaded into the Carius tube. Subsequent to that, $^{185}Re$ and $^{190}Os$ spikes, 6 mL 10 mol $l^{-1}$ HCl and 18 ml 15 mol $l^{-1}$ $HNO_3$ were added into 100 mL Carius tube consequently while the tube was immersed in an ethanol-liquid nitrogen slush. After the bottom part of the tube was frozen, the top of the tube was sealed under partial vacuum using an oxygen-propane torch. The tube was then placed in a stainless-steel jacket and heated to 230 °C for at least 48 h for complete dissolution and homogenization of the sample and spike. After the solution had cooled down, the tube was kept frozen, and the neck was carefully broken. 40 mL Milli-Q water was added from the neck hole into the tube. The top of each Carius tube was sealed with a stretchy rubber head of a dropper. Thereafter, thin Teflon tubes were inserted through two holes in the upper part of the rubber head, serving as inlet and outlet for clean air and $OsO_4$ vapor, respectively. The Os was separated as $OsO_4$ from the solution by distillation in the steam bath, and trapped in 2 ml ice water for Os isotope ratio determination. Re was extracted from the aqueous residue by column chromatography using an anionic resin (AG1x8 100–200 mesh). Both Os and Re isotope ratios were determined using high resolution inductively coupled plasma spectrometer (Element 1 ICP-MS). The error for the ages was reported as 1.02%, which represents a combination of measurement errors, the Re decay constant error, and spike calibrations. The decay constant used for $^{187}Re$ was $1.666 \times 10^{-11}$ $year^{-1}$ (Smoliar et al., 1996). The contribution of the

**Table 1**
Re-Os isotopic data for chalcopyrite from the Xiaotongchang Cu deposit.

| Sample no. | Orebody no. | Re ppb | $^{187}$Re ppb | Common Os ppt | $^{187}$Os ppt | $^{187}$Re/$^{188}$Os | $^{187}$Os/$^{188}$Os | Age Ma |
|---|---|---|---|---|---|---|---|---|
| XTC1-1 | 1 | 34.2 ± 0.2 | 21.5 ± 0.2 | 1.07 ± 0.13 | 82.5 ± 0.6 | 154,283 ± 18,574 | 591 ± 71 | 229.6 ± 3.2 |
| XTC1-2 | 1 | 21.0 ± 0.2 | 13.2 ± 0.1 | 0.57 ± 0.07 | 50.5 ± 0.4 | 178,142 ± 21,046 | 682 ± 80 | 229.4 ± 3.3 |
| XTC1-3 | 1 | 23.7 ± 0.2 | 14.9 ± 0.1 | 0.94 ± 0.09 | 57.7 ± 0.4 | 122,329 ± 11,896 | 473 ± 46 | 231.8 ± 3.3 |
| XTC1-4 | 1 | 70.1 ± 0.5 | 44.1 ± 0.3 | 3.2 ± 0.1 | 170 ± 1 | 105,535 ± 3568 | 406 ± 13 | 230.9 ± 3.4 |
| XTC1-5 | 1 | 84.1 ± 0.6 | 52.9 ± 0.4 | 1.6 ± 0.4 | 204 ± 2 | 258,197 ± 6768 | 997 ± 260 | 231.4 ± 3.4 |
| XTC1-6 | 1 | 86.2 ± 0.7 | 54.2 ± 0.4 | 6.5 ± 0.6 | 209 ± 1 | 64,084 ± 6254 | 247 ± 24 | 231.6 ± 3.4 |
| XTC1-7 | 1 | 22.0 ± 0.1 | 13.8 ± 0.1 | 2.17 ± 0.06 | 52.6 ± 0.1 | 48,743 ± 1531 | 186 ± 6 | 228.4 ± 3.5 |
| XTC1-8 | 1 | 27.0 ± 0.2 | 17.0 ± 0.1 | 8.80 ± 0.05 | 65.4 ± 0.4 | 23,516 ± 1683 | 56 ± 7 | 231.1 ± 3.1 |
| XTC3-1 | 3 | 4.42 ± 0.04 | 2.78 ± 0.03 | 0.614 ± 0.036 | 10.8 ± 0.2 | 34,740 ± 2054 | 135 ± 8 | 234.4 ± 5.0 |
| XTC3-2 | 3 | 3.66 ± 0.03 | 2.30 ± 0.02 | 0.503 ± 0.001 | 8.76 ± 0.05 | 34,902 ± 1889 | 132 ± 15 | 229.1 ± 3.1 |
| XTC3-3 | 3 | 5.65 ± 0.07 | 3.55 ± 0.04 | 0.815 ± 0.013 | 13.7 ± 0.1 | 33,495 ± 672 | 129 ± 2 | 231.6 ± 4.0 |
| XTC3-4 | 3 | 1.17 ± 0.01 | 0.736 ± 0.005 | 0.230 ± 0.016 | 2.84 ± 0.02 | 34,352 ± 1524 | 135 ± 6 | 231.1 ± 3.1 |
| XTC3-5 | 3 | 2.98 ± 0.02 | 1.87 ± 0.02 | 0.205 ± 0.005 | 7.32 ± 0.05 | 70,241 ± 1831 | 275 ± 7 | 234.6 ± 3.4 |
| JCBY | | 38.55 ± 0.51 | | 15.93 ± 0.08 | 0.6918 ± 0.0051 | | 0.3355 ± 0.0021 | |
| certified value | | 38.61 ± 0.54 | | | | | 0.3363 ± 0.0029 | |

blanks of Re was 2.3 ± 0.6 pg and Os 0.43 ± 0.16 pg.

### 3.2. Sulfur isotope analysis

Sulfur isotope analyses were performed on pure chalcopyrite powder using a conventional off-line method. Approximately 5 mg of chalcopyrite was homogenized with 40 mg of $V_2O_5$, and combusted at 940 °C for 30 min under vacuum for a quantitative conversion to sulfur dioxide ($SO_2$). After that, the sample was analyzed for sulfur isotope composition on a Finnigan DELTA S gas source mass spectrometer. Sulfur isotope ratios are expressed as per mil (‰) deviations from the sulfur isotope composition of Vienna-Canyon Diablo Troilite (VCDT), using the conventional delta ($\delta^{34}S$) notation. Pyrite (LTB-2) was used as internal standard. The reproducibility of $\delta^{34}S$ values are within ± 0.2‰.

### 3.3. Trace elements analysis

Both chalcopyrite and basalt samples were decomposed by HCl-$HNO_3$ solution under high pressure at 200 °C for 5 days. The trace elements in the final 2% $HNO_3$ solution were determined by HR-ICP-MS (Element I). The uncertainty in the analysis was less than ± 8%.

### 3.4. Analysis of $Cl^-$ in fluid inclusions

Quartz and calcite minerals separated from the samples were decomposed by HCl solution at room temperature for 3 days. The content of $Cl^-$ in the fluid inclusions was determined by single-channel ion chromatography.

## 4. Results

### 4.1. Chalcopyrite Re-Os isotopes

The data for the 13 chalcopyrite samples from the No. 1 and 3 ore bodies of the Xiaotongchang Cu deposit are listed in Table 1. All the chalcopyrite samples have Re abundances ranging from ~1 to about 86 ppb (Table 1). There are wide variations in Re contents among the separates from individual deposits. Chalcopyrite samples from the No. 1 ore body contain 21–86 ppb Re and 50–210 ppt $^{187}$Os, while those from the No. 3 ore body contain 1.1–5.7 ppb Re and 2.8–13.7 ppt $^{187}$Os. These 13 chalcopyrite samples have low content of common Os, ranging from 0.2 to 8.8 ppt. Radiogenic $^{187}$Os ($^{187}Os^r$) thus, accounts for > 90% of the total $^{187}$Os budget, except XTC1-8 with 88% (Table 1). All the samples have extremely high $^{187}$Re/$^{188}$Os (up to $2.3 \times 10^4$), whilst the $^{187}$Os/$^{188}$Os ratios are in excess of 50. The dominance of radiogenic Os and high $^{187}$Re/$^{188}$Os are diagnostic features of "LLHR"

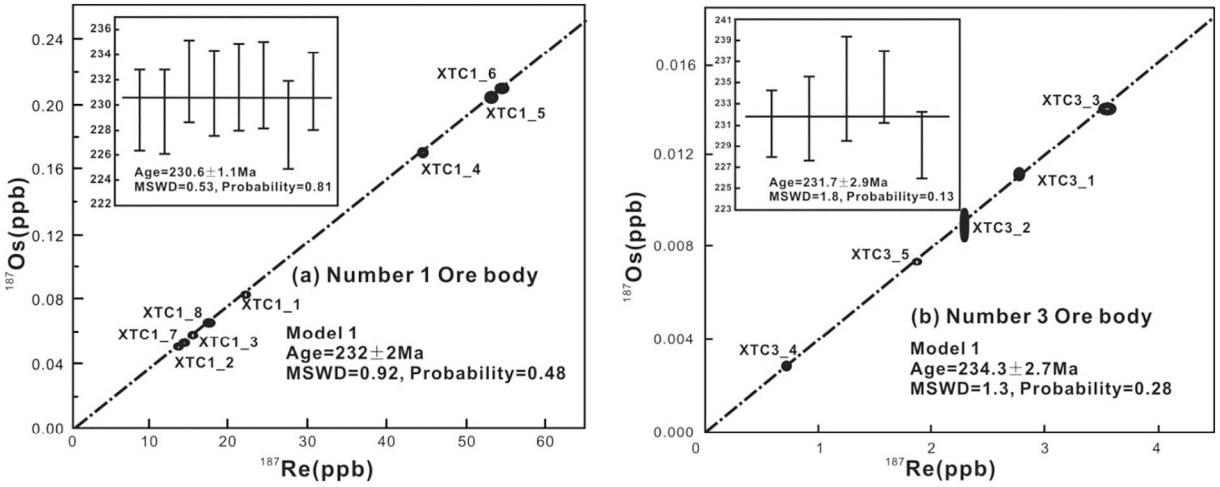


**Fig. 5.** $^{187}$Re-$^{187}$Os (parent-daughter) isochron diagrams and weighted average model age diagrams for chalcopyrite samples. (a) No. 1 ore body in Xiaotongchang deposit. (b) No. 3 ore body in Xiaotongchang deposit.

**Table 2**
Sulfur isotope data of chalcopyrite samples from both ore body in Xiaotongchang deposit.

| Sample no. | Orebody no. | $\delta^{34}S$(‰) | Sample no. | Orebody no. | $\delta^{34}S$(‰) |
|---|---|---|---|---|---|
| XTC1_5 | Body 1 | 8.4 | XTC3_1 | Body 3 | 9.5 |
| XTC1_6 | Body 1 | 9.2 | XTC3_2 | Body 3 | 8.8 |
| JM10_152[a] | Body 1 | 7.4 | XTC3_3 | Body 3 | 8.3 |
| JM10_17[a] | Body 1 | 8.2 | XTC3_4 | Body 3 | 9.1 |
| JM10_166[a] | Body 1 | 7.7 | XD-5-3-1[a] | Body 3 | 8.5 |
| ave | Body 1 | 8.2 | ave | Body 3 | 8.8 |

[a] Data from Shen (Shen, 2013).

(low-level, highly radiogenic) sulfides (Stein et al., 2000; Cardon et al., 2008). Accordingly, the best way to display the results is to plot the radiogenic $^{187}Os$ against $^{187}Re$ rather than the $^{187}Re/^{188}Os$ versus $^{187}Os/^{188}Os$, because the extremely low $^{188}Os$ contents, compared to the blank contribution, have resulted in inaccurate $^{187}Os/^{188}Os$ ratios. The copper-nickel-sulfide standard JCBY used in this study yielded a mean value of 0.3355 ± 0.0021 for $^{187}Os/^{188}Os$ compared with the certified value of 0.3363 ± 0.0021 (Qu et al., 2009).

The eight chalcopyrite separates from the No. 1 ore body yield model ages ranging from 229.4 ± 3.3 to 231.8 ± 3.4 Ma, with a weighted average model age of 230.6 ± 1.1 Ma and a MSWD of 0.53. These sample also produce a well-constrained $^{187}Re$-$^{187}Os$ isochron age of 232 ± 2 Ma (MSWD = 0.92) (Fig. 5). Both ages are the same within analytical uncertainty, but the more precise estimate from the model age is our preferred age.

As in the case of the other five separates from the No. 3 ore body, the Re-Os model ages range from 229.1 ± 3.1 to 234.4 ± 5.0 Ma, and the weighted average of the five analyses is 231.7 ± 2.9 Ma, with a MSWD of 1.3 (Fig. 5). A direct regression of $^{187}Re$ against $^{187}Os$ yielded a slightly older age of 234.3 ± 2.7 Ma (MSWD = 1.8). The weighted average of the model age which is not easily influenced by the maximum age, is our preferred age.

### 4.2. Sulfur isotope

The $\delta^{34}S$ values for the chalcopyrite samples from the No. 1 ore body in Xiaotongchang deposit vary from 7.4 to 9.2‰, with an average value of 8.2‰ (Table 2). For sulfide minerals from the No. 3 ore body, the $\delta^{34}S$ values vary from 8.3 to 9.5‰, with an average value of 8.8‰ (Table 2).

### 4.3. Rare earth elements

The analytical results for the rare earth elements (REEs) and other details are presented in Table 3. The chondrite-normalized (Boynton, 1984) REEs patterns for basalt, chalcopyrite and limestone samples are shown in Fig. 6(a). For a better understanding of the general behavior of the REEs, their average compositions in the respective samples are presented in Fig. 6(b). Here, the REEs in the basalts have higher concentration (> 60 ppm) compared with those in the chalcopyrites and limestones. The pattern of basalt shows slight enrichment in LREE ($La_N/Yb_{N\_ave}$ = 3.26), predominantly no Eu anomalies ($Eu/Eu^*_{\_ave}$ = 0.95) and no negative Ce anomalies ($Ce/Ce^*_{\_ave}$ = 0.93). On the contrast, the REE pattern of Maokou Formation limestone (Xiao, 2005) displays the distinct behavior as exceptionally negative Ce anomalie ($Ce/Ce^*_{\_ave}$ = 0.33) and Eu anomalie ($Eu/Eu^*_{\_ave}$ = 0.58) and enrichment in LREE to HREE ($La_N/Yb_{N\_ave}$ = 14.7). All the chalcopyrite separates show low REE contents (1.1–1.2 ppm), strong fractionation between the LREE and HREE ($La_N/Yb_N$ = 8.5) and negative Ce anomalies ($Ce/Ce^*$ = 0.66–0.76). Specifically, the chalcopyrites from the No. 1 ore body display no Eu anomalies ($Eu/Eu^*_{\_ave}$ = 1.05), while those from No. 3 ore body show weak negative Eu anomalies ($Eu/Eu^*_{\_ave}$ = 0.80).

**Table 3**
Rare earth elements concentrations (ppm) of ore and wallrock in the Xiaotongchang deposit.

| | B-1 | B-2 | B-ave | XTC1-4 | XTC1-5 | XTC1-6 | XTC1-ave | XTC3-2 | XTC3-3 | XTC3-4 | XTC3-ave | $P_2m$-1[a] | $P_2m$-2[a] | $P_2m$-ave |
|---|---|---|---|---|---|---|---|---|---|---|---|---|---|---|
| | Basalt | | | cpy_ore1 | | | | cpy_ore3 | | | | Limestone | | |
| La | 11.1 | 9.20 | 10.2 | 0.451 | 0.165 | 0.273 | 0.296 | 0.230 | 0.356 | 0.241 | 0.276 | 2.03 | 3.31 | 2.67 |
| Ce | 23.4 | 19.8 | 21.6 | 0.599 | 0.193 | 0.327 | 0.373 | 0.404 | 0.596 | 0.272 | 0.424 | 1.51 | 1.42 | 1.47 |
| Pr | 3.33 | 2.89 | 3.11 | 0.089 | 0.025 | 0.053 | 0.056 | 0.055 | 0.08 | 0.044 | 0.060 | 0.33 | 0.40 | 0.37 |
| Nd | 14.9 | 13.6 | 14.3 | 0.392 | 0.084 | 0.185 | 0.220 | 0.219 | 0.325 | 0.184 | 0.243 | 1.31 | 1.55 | 1.43 |
| Sm | 4.06 | 3.59 | 3.83 | 0.084 | 0.019 | 0.04 | 0.048 | 0.056 | 0.066 | 0.045 | 0.056 | 0.24 | 0.37 | 0.31 |
| Eu | 1.41 | 1.05 | 1.23 | 0.028 | 0.007 | 0.013 | 0.016 | 0.015 | 0.016 | 0.012 | 0.014 | 0.05 | 0.07 | 0.06 |
| Gd | 4.33 | 3.82 | 4.08 | 0.076 | 0.017 | 0.039 | 0.044 | 0.056 | 0.063 | 0.041 | 0.053 | 0.29 | 0.37 | 0.33 |
| Tb | 0.715 | 0.696 | 0.706 | 0.013 | 0.003 | 0.006 | 0.007 | 0.009 | 0.010 | 0.006 | 0.008 | 0.04 | 0.06 | 0.05 |
| Dy | 4.50 | 4.29 | 4.40 | 0.079 | 0.017 | 0.037 | 0.044 | 0.050 | 0.058 | 0.039 | 0.049 | 0.26 | 0.37 | 0.32 |
| Ho | 0.881 | 0.891 | 0.886 | 0.016 | 0.004 | 0.007 | 0.009 | 0.009 | 0.011 | 0.008 | 0.009 | 0.07 | 0.08 | 0.075 |
| Er | 2.33 | 2.48 | 2.41 | 0.046 | 0.011 | 0.020 | 0.026 | 0.023 | 0.026 | 0.024 | 0.024 | 0.20 | 0.20 | 0.20 |
| Tm | 0.332 | 0.375 | 0.354 | 0.007 | 0.002 | 0.003 | 0.004 | 0.003 | 0.004 | 0.004 | 0.004 | 0.03 | 0.03 | 0.03 |
| Yb | 2.08 | 2.39 | 2.24 | 0.046 | 0.011 | 0.018 | 0.025 | 0.020 | 0.023 | 0.028 | 0.024 | 0.13 | 0.13 | 0.13 |
| Lu | 0.308 | 0.365 | 0.337 | 0.007 | 0.002 | 0.003 | 0.004 | 0.003 | 0.004 | 0.005 | 0.004 | 0.02 | 0.03 | 0.025 |
| ΣREE | 73.6 | 65.3 | 69.5 | 1.93 | 0.56 | 1.02 | 1.17 | 1.15 | 1.64 | 0.95 | 1.25 | 6.51 | 8.39 | 7.45 |
| Eu/Eu* | 1.02 | 0.86 | 0.95 | 1.05 | 1.17 | 0.99 | 1.07 | 0.81 | 0.75 | 0.84 | 0.80 | 0.58 | 0.57 | 0.58 |
| Ce/Ce* | 0.93 | 0.93 | 0.93 | 0.69 | 0.66 | 0.63 | 0.66 | 0.85 | 0.83 | 0.60 | 0.76 | 0.41 | 0.26 | 0.33 |
| $(La/Yb)_{SN}$ | 3.83 | 2.76 | 3.26 | 7.03 | 10.8 | 10.9 | 8.50 | 8.25 | 11.1 | 6.17 | 8.51 | 11.2 | 18.3 | 14.7 |

$Eu/Eu^* = 2 \times (Eu)_{SN}/(Sm_{SN} + Gd_{SN})$; $Ce/Ce^* = 2 \times (Ce)_{SN}/(La_{SN} + Pr_{SN})$.
[a] Data for limestone from Xiao (Xiao, 2005).

### 4.4. $Cl^-$ composition of fluid inclusions in quartz and calcite

Quartz and calcite minerals associated with chalcopyrite in the No. 1 and 3 ore bodies were analyzed for their $Cl^-$ composition, and the results are presented in Table 4. The $Cl^-$ concentrations in the quartz-hosted fluid inclusions (No. 1 ore body: 19.1–33.5 ppm; No. 3 ore body 14.6–24.3 ppm; average 21.3 ppm) are much higher than in the calcite-hosted fluid inclusions (No. 1 ore body: 3.4–6.7 ppm; No. 3 ore body: 2.7–8.4 ppm; average 5.0 ppm).

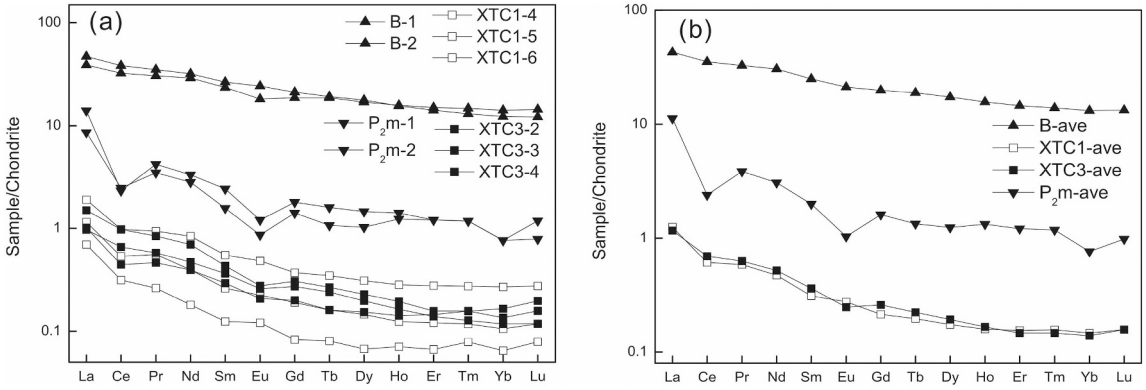


**Fig. 6.** Chondrite-normalized REE profiles for basalts (B-1 and B-2), chalcopyrites (XTC1 from No. 1 ore body, XTC3 from No. 3 ore body) and limestone ($P_2m$) from the Maokou formation (Xiao, 2005). (a) Pattern for each individual sample; (b) pattern for average REEs of each type samples.

## 5. Discussion

### 5.1. Source of ore-forming materials and fluids

The chalcopyrite is devoid of non-metallic mineral inclusions, and therefore, it could represent the characteristic of the ore-forming fluids. The high Cu content in the basalt, consistent with earlier research on basalt-related Cu ore from northeastern Yunnan (Li et al., 2004; Shen, 2013), indicate that the basalt could be the main ore-forming material.

The Chondrite-normalized distribution patterns of REE in Xiaotongchang chalcopyrite samples display negative Ce anomalies (Ce/Ce* = 0.60–0.83) and LREE enrichment relative to HREE ($(La/Yb)_{SN}$ = 6.17–11.10). This value is between basalt ($(La/Yb)_{SN}$ = 3.26, Ce/Ce* = 0.93) and limestone ($(La/Yb)_{SN}$ = 14.7, Ce/Ce* = 0.33). In details, the chalcopyrite samples show weak negative Eu anomalies in No.3 body (Eu/Eu* = 0.75-0.84) and no Eu anomaly (Eu/Eu* = 0.99-1.17) in No. 1 body (Table 3, Fig. 6). Hence, this implies that the limestone has much more influence on the sources of ore-forming fluids in No.3 ore body. This behavior is according with the appearance that calcite was the mainly associated mineral in No. 3 ore body. Combined with the C isotope analysis on calcite (Shen, 2013), we proposed that calcite in this region may have been derived from pyrolysis process of the Permian Maokou limestone.

Chalcopyrites are the major sulfide mineral assemblage in the Xiaotongchang deposit. Therefore, the sulfide $\delta^{34}S$ values can act as a proxy for the $\delta^{34}S$ values of the ore-forming fluids (Basuki et al., 2008; Dixon and Davidson, 1996). All the sulfide separates from the Xiaotongchang have $\delta^{34}S_{CDT}$ values ranging from +7.4‰ to +9.5‰ (Table 2). Claypool *et al.* (1980) and Taylor (1983) suggested that Late Permian seawater sulfate has a distinctive $\delta^{34}S$ range around +10.5 ± 1.0‰. The Emeishan basalt in Jinping area has a distinctive $\delta^{34}S$ with 4.84‰ (Zhang, 2006). As a result, it is indicated that the S isotopic composition of the Xiaotongchang is between the basalt and limestone.Therefore, this study suggests that the ore-forming materials were most likely derived from a mixture of basalt and stratum components.

**Table 4**
$Cl^-$ concentrations (in ppm) in inclusions in quartz and calcite associated with the chalcopyrite from both ore bodies in the Xiaotongchang deposit.

| | No. 1 ore body | | No. 3 ore body | |
|---|---|---|---|---|
| Quartz | XTC1-a-Q | 33.5 | XTC3-a-Q | 24.3 |
| | XTC1-c-Q | 19.1 | XTC3-b-Q | 16.7 |
| | XTC1-e-Q | 19.7 | XTC3-e-Q | 14.6 |
| Calcite | XTC1-a-C | 6.68 | XTC3-a-C | 2.66 |
| | XTC1-c-C | 3.75 | XTC3-b-C | 8.39 |
| | XTC1-e-C | 3.36 | XTC3-e-C | 5.12 |

### 5.2. Variations in the Re concentrations and application of LLHR sulfide

Chalcopyrite from the No. 1 and 3 ore bodies are classed as LLHR sulfides (i.e. $^{187}Re/^{188}Os > 5000$ and $> 80\%^{187}Os^R$ (Stein et al., 2000). It is worthy to note that the Re contents of these chalcopyrite separates from the individual copper deposits vary by about one order of magnitude. A similar situation also can be found in the neighboring gold deposits, namely, Stog'er Tight and Pine Cove (Kerr and Selby, 2012).

In order to make sense of the data, we explore some potential causes of the wide variation in Re concentration.

A) LLHR-type sulfide like molybdenite could be controlled by micro-intergrowths of molybdenite within Cu-sulfides (Selby et al., 2009).

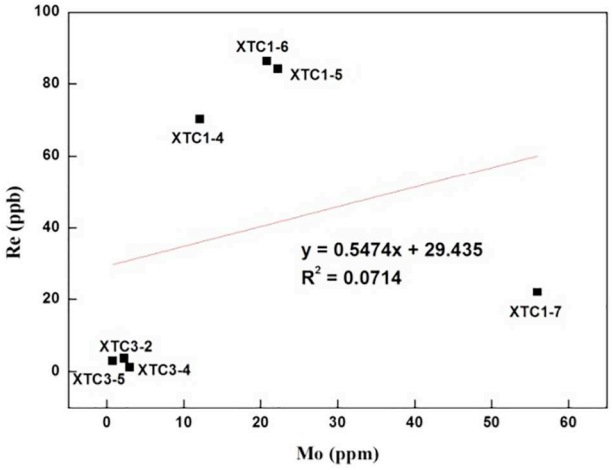


**Fig. 7.** Re vs. Mo diagram for chalcopyrite samples from the No. 1 and 3 ore bodies in the Xiaotongchang deposit.

However, no molybdenite was found in our samples, either in hand specimen or observation under petrographic microscope and scanning electron microscope (SEM). Simultaneously, the Mo contents in seven chalcopyrite samples from the both ore body are < 60 ppm, and they display no linear relationship with the Re content by $R^2 = 0.07$ (Fig. 7). Therefore, it is suggested that the similar geochemical behavior of Mo and Re is not the main reason for variation of Re.

B) Re is preferentially trapped in Ge-enriched minerals, like germanite and renierite to elevate the Re concentration, and therefore has strong correlations with Co, Ni, Cu, and Ge (Selby et al., 2009; Stein et al., 2001). The studied chalcopyrite separates are known to contain very low Ge content (5 ppm, unpub data), and Co, whereas Ni does not appear to contain elevated Re (unpub data). Therefore, this possibility could be excluded as the cause of the large Re variation.

C) Based on experimental studies, Xiong and Wood (1999) suggested Re is strongly dependent on pH and $Cl^-$ concentration. In this study, the content of $Cl^-$ in the quartz-hosted fluid inclusions (average 21.3 ppm) in the No. 1 and No. 3 ore bodies is higher than the content in the calcite-hosted fluid inclusions (average 5.0 ppm) in both ore bodies (Table 4). As mentioned above, the quartz is more observed in the chalcopyrite separates from No. 1 ore body, whereas, calcite is the dominant gangue mineral in the chalcopyrite separates from the No. 3 ore body. Hence, the Re enrichment observed the No. 1 copper ore body can be ascribed to the effect of $Cl^-$ content on the variations in the Re concentrations.

To summarize, evidence of variations in the Re concentrations in the Xiaotongchang deposit is explained by the relationship between Re and $Cl^-$.

### 5.3. Age of copper mineralization and its relation to evolution of the Aliaoshan orogen

Our first precise Re-Os ages of chalcopyrites provide constraints on the timing of the formation of the Xiongtongchang Cu deposit. All the chalcopyrites from No. 1 and 3 ore bodies in the Xiaotongchang Cu deposit are classified as LLHR sulfides. In view of these attributes, the weighted averages of the Re-Os model ages are considered to give the best estimate of the timing of the chalcopyrite formation. These results indicate ages of 230.6 ± 1.1 Ma for No. 1 ore body and 231.7 ± 2.9 Ma for No. 3 ore body, which overlap within their respective analytical uncertainties. The mean model age also overlaps the less precise estimates obtained through regression of $^{187}Re$ against $^{187}Os$ (232 ± 2 Ma and 234.3 ± 2.7 Ma, respectively). These results indicate that both ore bodies are coeval within the resolution of our technique. Because the higher Re concentration and more precise Re-Os age were obtained from the No. 1 ore body and the chalcopyrite was the primary copper mineral, the Re−Os chalcopyrite average model age of 230.6 ± 1.1 Ma is interpreted to represent the age of Cu mineralization in the Xiaotongchang deposit, suggesting that the deposit was formed during the Middle Triassic. Therefore, the age of Xiaotongchang deposit differs from the porphyry-type deposit forming during the collision setting between the Indian plant and Eurasian plant in Himalayan period (He *et al.*, 2011) and copper-nickel sulfide deposits with the age close to the major eruption stage of the Emeishan large igneous provinces (Shi *et al.*, 2006)

Simultaneously , some metal deposits were formed in the northwest section of the Ailaoshan metallogenic belt during the Middle Triassic, such as Yangla copper deposit (227 Ma, U-Pb) (Li *et al.*, 2014) and Zhenyuan gold deposit (229 ± 38 Ma, Re-Os) (Shi *et al.*, 2012). Whereas, few Triassic deposits had been discovered in the southeast section of the Ailaoshan metallogenic belt before. Therefore, the age discovery of Xiaotongchang deposit provides new information for reginonal tectonic evolution in the southeast section of the Ailaoshan metallogenic belt.

Previous studies (Zhang *et al.*, 1999; Ge *et al.*, 2010; Zhong *et al.*, 2001) have shown that in the early period of the Late Permian, the crust of the Ailaoshan area was splitted, resulting in the eruption of basalt and the formation of an unconformable contact with the overlying Early Permian limestone. The petrology and geochemistry of the basalts showed that the rift was formed on the edge of the Yangtze plate. Similar rift can be found in the northern part of the region (Zhang *et al.*, 1999), suggesting that, the crustal break-up was most likely caused by the subduction orogenic event. Furthermore, the time of basalt eruption was consistent with the formation time of the Emeishan large igneous province (Ge *et al.*, 2010). Until the early Triassic period, the Ailaoshan ocean was completely closed, while the Yangtze plate had thrusted over the Lanping-Simao block, leading to the formation of the Ailaoshan orogene (Wei and Shen, 1997; Zhong *et al.*, 2001). During late the collision orogenesis some interlayer fracture zone and faults were formed in the Jinping basalt distributed region.

## 6. Conclusion

This study demonstrates that Re-Os geochronological studies of chalcopyrites associated with vein Cu deposit in basalts at Xiaotongchang deposit can yield useful and precise age information for No. 1 and No. 3 ore bodies. Due to the extremely low concentration of the common Os, the chalcopyrites are qualified as LLHR sulfides, amenable to model age calculations. However, it can be seen that the Re contents in chalcopyrite samples from the No. 1 ore body is higher than those in No. 3 ore body by an order of magnitude. A possible explanation is that $Cl^-$ in the fluid inclusions of the associated gangue minerals is the factor to highly enrich in Re.

The yielded Re-Os data have firstly provided the absolute ages (230.6 ± 1.1 Ma) of ore formation for the Xiaotongchang Cu deposit. Based on geological and geochronological evidences, we suggest that the Xiaotongchang Cu deposit resulted from the late collision setting of the Ailaoshan orogenic evolution during Indosinian movement. The results of the trace element and S isotope indicate that the ore-forming materials were derived from a mixture of mantle (Emeishan basalt) and crustal components (stratum).

## Acknowledgements

This work was jointly financially supported by the National Natural Science Foundation of China (NSFC 41503056, 41603016).

## References

Basuki, N.I., Taylor, B.E., Spooner, E.T., 2008. Sulfur Isotope Evidence for Thermochemical Reduction of Dissolved Sulfate in Mississippi Valley-Type Zinc-Lead Mineralization, Bongara Area, Northern Peru. Econ. Geol. 103, 783–799.

Boynton, W.V., 1984. Cosmochemistry of the rare earth elements: meteorite studies. Developments in geochemistry 2. Elsevier, pp. 63–114.

Cai, Y.F., Wang, Y.J., Cawood, P.A., Fan, W.M., Liu, H.C., Xing, X.W., Zhang, Y.Z., 2014. Neoproterozoic subduction along the Ailaoshan zone, South China: Geochronological and geochemical evidence from amphibolites. Precambrian Res. 245, 13–28.

Cardon, O., Reisberg, L., Andre-Mayer, A.S., Leroy, J., Milu, V., Zimmermann, C., 2008. Re-Os systematics of pyrite from the Bolcana porphyry copper deposit, Apuseni mountains, Romania. Econ. Geol. 103, 1695–1702.

Chen, D., 2015. Comparison of the Basalt Copper Deposits in the Keweenaw Peninsula of Michigan (USA) and the Adjacent Area of Yunnan-Guizhou Provinces (China). Geotecton. Metallog. 39, 110–127 (in Chinese with English abstract).

Claypool, G.E., Holser, W.T., Kaplan, I.R., Sakai, H., 1980. The age curve of sulphur and oxygen bisotopes in marine sulphate and their mutual interpretation. Chem. Geol. 56, 1594–1599.

Dai, C.G., Liu, A.M., Wang, M., Wu, G.R., 2004. Characteristic and Mineralization of Emeishan Basaltic Copper Deposits in the West of Guizhou Province. Guizhou Geol. 21, 71–75 (in Chinese with English abstract).

Deng, X.H., Wang, J.B., Pirajno, F., Wang, Y.W., Li, Y.C., Li, C., Zhou, L.M., Chen, Y.J., 2016. Re-Os dating of chalcopyrite from selected mineral deposits in the Kalatag district in the eastern Tianshan Orogen, China. Ore Geol. Rev. 77, 72–81.

Dixon, G., Davidson, G.J., 1996. Stable isotope evidence for thermochemical sulfate reduction in the Dugald river (Australia) strata-bound shale-hosted zinc lead deposit.

Chem. Geol. 129, 227–246.
Ge, L.S., Deng, J., Yang, L.Q., 2010. Evolution of tectonic environment and gold-polymetal metallogenic system in ailaoshan ore concentration region, yunnan province, china. Acta Petrol. Sin. 26, 1699–1722 (in Chinese with English abstract).
He, W.Y., Mo, X.X., Yu, X.H., Li, Y., Huang, X.K., He, Z.H., 2011. Geochronological study of magmatic intrusions and mineralization of machangqing porphyry Cu-Mo-Au deposit, western yunnan province. Earth Sci. Front. 141, 39–48 (in Chinese with English abstract).
Huang, X.W., Zhou, M.F., Beaudoin, G., Gao, J.F., Qi, L., Lyu, C., 2018. Origin of the volcanic-hosted Yamansu Fe deposit, Eastern Tianshan, NW China: constraints from pyrite Re-Os isotopes, stable isotopes, and in situ magnetite trace elements. Mineral. Deposita 1–22.
Jin, X.D., Li, W.J., Xiang, P., Sakyi, P.A., Zhu, M.T., Zhang, L.C., 2013. A contribution to common Carius tube distillation techniques. J. Anal. At. Spectrom. 28, 396–404.
Kelley, K.D., Selby, D., Falck, H., Slack, J.F., 2017. Re-Os systematics and age of pyrite associated with stratiform Zn-Pb mineralization in the Howards Pass district, Yukon and Northwest Territories, Canada. Mineral. Deposita 52, 317–335.
Kerr, A., Selby, D., 2012. The timing of epigenetic gold mineralization on the Baie Verte Peninsula, Newfoundland, Canada: new evidence from Re–Os pyrite geochronology. Mineral. Deposita 47, 325–337.
Li, L.W., 2009. Geological features, ore-forming geological conditions and direction of prospecting of Cu-polymetallica deposit in Yunnan Jinping. Dissertation. Kunming University of Science and Technology, China.
Li, J., Chen, W., Yong, Y., Yang, L., Liu, Y.D., Luo, C., Sun, J.B., Zhang, B., 2014. Genesis and metallogenice epoch of Yangla copper deposit, Yunnan Province. Acta Petrol. Sin. 30 (8), 2269–2278 (in Chinese with English abstract).
Li, H.M., Mao, J.W., Xu, Z.B., Chen, Y.C., Zhang, C.Q., Xu, H., 2004. Copper mineralization characteristics of the Emeishan basalt district in the Yunnan-Guizhou border area. Acta Geosci. Sin. 25, 495–502 (in Chinese with English abstract).
Luo, X., Li, Y.S., Guo, N.N., Xie, Y., Cheng, X.Y., Zuo, T., 2011. Analysis of mineralization condition about a copper deposit in Jinping, Yunnan. Nonferrous Met. (Min. Sect.) 63, 31–33 (in Chinese with English abstract).
Nozaki, T., Kato, Y., Suzuki, K., 2010. Re–Os geochronology of the Iimori Besshi-type massive sulfide deposit in the Sanbagawa metamorphic belt, Japan. Geochim. Cosmochim. Acta 74, 4322–4331.
Qu, W.J., Du, A.D., Li, C., Sun, W.J., 2009. High-precise Determination of Osmium Isotopic Ratio in the Jinchuan Copper-Nickel Sulfide Ore Samples. Rock Miner. Anal. 28, 219–222 (in Chinese with English abstract).
Selby, D., Kelley, K.D., Hitzman, M.W., Zieg, J., 2009. Re–Os sulfide (bornite, chalcopyrite, and pyrite) systematics of the carbonate-hosted copper deposits at Ruby Creek, southern Brooks range, Alaska. Econ. Geol. 104, 437–444.
Shen, X.L., 2013. Research on the Permian mafic magma mineralization in Honghe prefecture, Yunnan Province. Dissertation. Insistitute of Geology and Geophysics, Chinese Academy of Sciences.
Shi, G.Y., Sun, X.M., Pan, W.J., Hu, B.M., Qu, W.J., Du, A.D., 2012. Re-Os dating of auriferous pyrite from the Zhenyuan super-large gold deposit in Ailaoshan gold belt, Yunnan province, southwestern china. Sci. Bull. 57 (35), 4578–4586 (in Chinese with English abstract).
Shi, G.Y., Sun, X.M., Wang, S.W., Xiong, D.X., Qu, W.J., Du, A.D., 2006. Re-Os isotopic dating and its geological implication of Baimazhai Cu-Ni sulphide deposit, Yunnan province, china. Acta Petrol. Sin. 22, 2451–2456 (in Chinese with English abstract).
Smoliar, M.I., Walker, R.J., Morgan, J.W., 1996. Re-Os Ages of Group IIA, IIIA, IVA, and IVB Iron Meteorites. Science 271, 1099–1102.
Stein, H.J., Markey, R.J., Morgan, J.W., Hannah, J.L., Scherstén, A., 2001. The remarkable Re-Os chronometer in molybdenite: how and why it works. Terra Nova 13, 479–486.
Stein, H.J., Morgan, J.W., Scherstén, A., 2000. Re-Os dating of low-level highly radiogenic (LLHR) sulfides: The Harnäs gold deposit, Southwest Sweden, Records Continental-Scale Tectonic Events. Econ. Geol. 95, 1657–1671.
Taylor, R.S., 1983. A stable study of the Mercia Mudstones (Keuper Marl) and associated sulphate horizons in the English Midlands. Sedimentology 30, 11–31.
Torgersen, E., Viola, G., Sandstad, J.S., Stein, H., Zwingmann, H., Hannah, J., 2015. Effects of frictional–viscous oscillations and fluid flow events on the structural evolution and Re–Os pyrite-chalcopyrite systematics of Cu-rich carbonate veins in northern Noway. Tectonophsics 659, 70–90.
Wang, M., Wang, W., Gutzmer, J., Liu, K., Li, C., Michałak, P.P., Guo, X., 2015. Re–Os geochronology on sulfides from the Tudun Cu–Ni sulfide deposit, Eastern Tianshan, and its geological significance. Int. J. Earth Sci. 104, 2241–2252.
Wei, Q.R., Shen, S.Y., 1997. Characteristics of three categories of arc volcanic rocks on the western side of Ailaoshan, Sanjiang area. Geol. Sci. Technol. Inf. 16, 13–18 (in Chinese with English abstract).
Xiao, J.F., 2005. The Evolution of the Mid-Proterozoic-Triassic Sedimentary basin and the element geochemical background of strata in SW margin of the Yangtze block. Dissertation. Insistitute of Geochemistry, Chinese Academy of Sciences.
Xiao, L., Xu, Y.G., Mei, H.J., He, B., 2003. Late Permian flood basalts at Jingping area and its relation to Emei mantl plume: geochemical evidence. Acta Petrol. Sin. 19, 38–48 (in Chinese with English abstract).
Xiong, Y., Wood, S.A., 1999. Experimental determination of the solubility of $ReO_2$ and the dominant oxidation state of rhenium in hydrothermal solutions. Chem. Geol. 158, 245–256.
Xu, J.F., Suzuki, K., Xu, Y.G., Mei, H.J., Li, J., 2007. Os, Pb, and Nd isotope geochemistry of the Permian Emeishan continental flood basalts: Insights into the source of a large igneous province. Geochim. Cosmochim. Acta 71, 2104–2119.
Yang, C.H., Wang, M.C., 2012. Cu metallogenesis rule of Emeishan basalt type of Mengla in Jingping, Yunnan. Yunnan Geol. 31, 177–181 (in Chinese with English abstract).
Ying, L.J., Wang, C.H., Tang, J.X., Wang, D.H., Qu, W.J., Li, C., 2014. Re–Os systematics of sulfides (chalcopyrite, bornite, pyrite and pyrrhotite) from the Jiama Cu–Mo deposit of Tibet, China. J. Asian Earth Sci. 79, 497–506.
Yuan, S.S., Ge, L.S., Lu, Y.M., Guo, X.D., Wang, M.J., Wang, Z.H., 2010. Relationship between crust-mantle reaction and gold mineralization in ailaoshan metallogenic belt: a case study of daping gold deposit in yuanyang. Mineral Deposits 29, 253–264 (in Chinese with English abstract).
Zeng, Q.D., Liu, J.M., Chu, S.X., Wang, Y.B., Sun, Y., Duan, X.X., Qu, W.J., 2014. Re-Os and U-Pb geochronology of the Duobaoshan porphyry Cu-Mo-(Au) deposit, northeast China, and its geological significance. J. Asian Earth Sci. 79, 895–909.
Zhang, X.S., 2006. Mafic-Ultramafic rocks, metallogenetic series and prospecting targeting in the Jinping-Songda rift. Dissertation. Kunming University of Science and Technology.
Zhang, P., Li, B., Li, J., Chai, P., Wang, X.J., Sha, D.M., Shi, J.M., 2016. Re-Os Isotopic Dating and its Geological Implication of Gold Bearing Pyrite from the Baiyun Gold Deposit in Liaodong Rift. Geotecton. Metallog. 40, 731–738 (in Chinese with English abstract).
Zhang, C., Qi, X.X., Tang, G.Z., Zhao, Y.H., Ji, F.B., 2014. Geochemistry and zircon U-Pb dating for the alkaline porphyries and its constraint on the mineralization in Chang'an Cu-Mo-Au ore concentration region, Ailaoshan orogenic belt, western Yunnan. Acta Petrol. Sin. 30, 2204–2216 (in Chinese with English abstract).
Zhang, Q., Qian, Q., Wang, Y., Xu, P., Han, S., Jia, X.Q., 1999. Late Paleozoic basic magmatism from SW Yangtze Massif and evolution of the Paleo-Tethyan Ocean. Acta Petrol. Sin. 15, 576–583 (in Chinese with English abstract).
Zhong, D.L., Ding, L., Liu, F.T., Liu, J.H., Zhang, J.J., Ji, J.Q., Chen, H., 2001. The polylayered architecture of lithosphere in the orogen and its constrain ton Cenozoic magmatism. Sci. China 30, 1–8 (in Chinese with English abstract).
Zhou, Q., Li, W.C., Zhang, H.H., Li, T.Z., Yuan, H.Y., Feng, X.L., Li, C., Liao, Z.W., Wang, S.W., 2017. Post-magmatic hydrothermal origin of late Jurassic Liwu copper polymetallic deposits, western China: Direct chalcopyrite Re-Os dating and Pb-B isotopic constraints. Ore Geol. Rev. 89, 526–543.